Engineering Geology 266 (2020) 105474

Contents lists available at ScienceDirect

Engineering Geology

journal homepage: www.elsevier.com/locate/enggeo

Automatic detection and characterisation of the first P- and S-wave pulse in rocks using ultrasonic transmission method

D. Benavente[a,*], J.J. Galiana-Merino[b], C. Pla[c], J. Martinez-Martinez[d], D. Crespo-Jimenez[e]

[a] Department of Earth and Environmental Sciences, University of Alicante, 3690 Alicante, Spain
[b] Department of Physics, Systems Engineering and Signal Theory, University of Alicante, 3690 Alicante, Spain
[c] Department of Civil Engineering, University of Alicante, 3690 Alicante, Spain
[d] Spanish Geological Survey, 28003 Madrid, Spain
[e] Department of Theoretical Physics and Cosmology, Science Faculty, University of Granada, 8071 Granada, Spain

ARTICLE INFO

Keywords:
Ultrasound
Nondestructive testing
Wavelet analysis
Building stones
Primary wave velocity
Shear wave velocity

ABSTRACT

In this paper, we propose a new methodology for the automatic picking of P- and S- wave arrivals. The measurement of elastic wave velocities is crucial for characterisation of the elastic properties of rocks, as well as their physico-mechanical properties and durability. P-waves are easy to generate and acquire, whereas the acquisition and subsequent analysis of the S-waves present major difficulties in most investigations of rocks.

In our proposed method the recorded signal is first pre-processed in the wavelet domain, removing low-frequency disturbances and filtering noise. The signal is then analysed in the time-domain to detect and characterise the first pulse and, subsequently, estimate the corresponding onset time. The automatic approach analyses all pulses detected in the output signal and selects the first pulse of the P or S wave relative to symmetry, amplitude and duration criteria. This triple check provides greater confidence in the obtained results.

We record P- and S- waveforms through the transmission method for a broad range of sedimentary, igneous and metamorphic rocks used in buildings. Results are compared to manual picking, which is considered as a true or reference value. The recorded signals show that microstructural components of rocks have a strong influence on the output signal. Mineralogical composition, porosity and particle size affect the wave velocity, attenuation, wavelength and waveform, which in turn influences the manual picking of the onset time.

The proposed methodology provides precise values of the onset time of P- and S- waves. The discrepancies between automatic and manual P- and S- wave picking are 0.7 and 4.4%, respectively. P-wave signals have a high signal-to-noise ratio and their arrival times are clear and easy to determine. However, the arrival time of S-waves presents significant problems, mainly for medium to coarse-grained rocks. In this case, the output signal is contaminated by P-waves and has a lower signal-to-noise ratio. Besides, propagation of the S-wave through the rock affects the frequency and waveform of the first pulse, which complicates manual picking of the onset time. The developed methodology distinguishes between the S-wave and the remaining P-waves contained in the transversal signal, independently of the skill and subjectivity of a human analyst.

1. Introduction

Methods based on elastic wave measurements are commonly used in engineering geology investigations. These non-destructive methods can be used in both laboratory and field experiments. In the laboratory, measurement of compressional and shear wave velocities is an excellent way to estimate the elastic characteristics of the studied materials, as well as their physico-mechanical and durability properties.

There are a number of factors that influence the elastic wave velocities of rocks. The most important determinants are the mineralogical content, texture, anisotropy, density, grain size and shape, porosity and pore and fissure size as well as water content, pressure and temperature (Hamdi and Lathaj, 2013; Brotons et al., 2016). Weathering of a rock also changes its elastic wave velocities by modification of its microstructural properties and also by the presence of water, precipitated salts, etc. (Benavente et al., 2018).

Elastic wave velocities are frequently investigated either individually or in combination. The compressional or primary (P) wave

* Corresponding author at: Department of Earth and Environmental Sciences, University of Alicante, Alicante, Spain.
E-mail addresses: david.benavente@ua.es (D. Benavente), jj.galiana@ua.es (J.J. Galiana-Merino), c.pla@ua.es (C. Pla), javier.martinez@igme.es (J. Martinez-Martinez), davidcrespo@ugr.es (D. Crespo-Jimenez).

https://doi.org/10.1016/j.enggeo.2020.105474
Received 19 June 2019; Received in revised form 31 December 2019; Accepted 1 January 2020
Available online 02 January 2020
0013-7952/

velocity, V_P, (also termed as ultrasonic pulse velocity) is the most commonly measured parameter, and is experimentally easy to estimate. The measurement technique used is characterised by strong penetration power and sensitivity that permits the non-destructive detection of petrographic defects inside rocks. In addition, P-wave velocity is used as indirect parameter for assessing rock strength and weathering. Shear or secondary (S) elastic wave velocity, V_S, is mostly obtained in combination with P-waves for the calculation of the Young and Poisson dynamic elastic moduli.

By analysing the recorded output waveform (mostly of the P-waves) more characteristics can be extracted such as waveform distortion, energy attenuation, frequency components, etc. These properties enhance information on rock microstructure obtained from wave velocities. For example, Martinez-Martinez et al. (2011, 2013) reported that spatial attenuation is much more sensitive to occasional rock defects (such as fissures and vuggy macropores) than wave velocity.

One of the most commonly used non-invasive methods to study the propagation of elastic waves through a material is the transmission method, where two piezoelectric sensors are coupled on either side of the material under study, one acting as an emitter and the other as a receiver. Experimentally, P-waves are easy to generate and acquire. Only in the case of weathered rock samples the generated waves could suffer a higher attenuation, producing output signals with a low signal-to-noise ratio (SNR). In contrast, the generation and acquisition of pure S-waves in rocks is difficult (Wang et al., 2009). In practice, normal incidence between the transducer and the sample is not perfectly accomplished, which produces also the transmission of compressional waves that might hide the S-waves. Thus, the picking of the onset time of the S-wave becomes a non-trivial process even for the most skilled analyst. In order to reduce the presence of longitudinal waves in the output signal, special normal incidence shear wave couplants of very high viscosity have to be used. However, complete removal of the couplant from the material under study after measurement is neither easy nor quick, thus considerably increasing the time required for each experiment. All of these difficulties serve to inhibit the measurement of S-waves and explain why calculation of the dynamic elastic moduli frequently considers a tabulated value of the Poisson's ratio, which yields an unrealistic determination of the elastic properties of rocks.

Once the output signal has been obtained, accurate determination of both elastic wave velocities, and therefore of the dynamic elastic moduli, is limited by accuracy of the picking of the onset time of each elastic wave. Manual picking is time-consuming and subjective according to the analyst who performs the picking. Manual operation requires careful attention by the skilled technician, which may be a disadvantage especially when a huge volume of data has to be analysed.

Hence, semi-automatic or automatic onset time picking methods are required for estimating elastic wave velocities. The most direct way is through the use of a PUNDIT (Portable Ultrasonic Nondestructive Digital Indicating Tester) instrument, which provides the propagation velocity of the ultrasonic pulse. In this case, a fixed threshold is used to determine the onset time of the P-waves, what makes it suitable only for signals with a relatively high SNR.

Alternatively, once the output signal has been recorded, a wide variety of first arrival picking techniques can be found in the literature, mostly inspired by geophysical methods. One of the most widespread approaches is the short-term average – long-term average (STA/LTA) ratio method (Allen, 1978; Earle and Shearer, 1994; Withers et al., 1998). In this case, the ratio between the average amplitudes of a short time window and a long time window is obtained and compared with a threshold. This technique is commonly used for picking the first arrival in signals with low noise level. An improvement to the STA/LTA method is achieved with the modified energy ratio (MER) method (Lee et al., 2017), which is more robust to background random noise.

Autoregressive techniques (Sleeman and van Eck, 1999; Leonard, 2000; Zhang et al., 2003; Kurz et al., 2005; Carpinteri et al., 2012) represent another approach for estimating the onset time based on the Akaike Information Criterion (AIC) (Akaike, 1974). In this case, the signal is assumed to be composed of two independent and locally stationary segments, just before and after the onset time, where the global minimum of the AIC function provides the separation point. The performance of the autoregressive AIC picker is better if the AIC is only applied to the part of the signal that contains the onset time (Zhang et al., 2003). In this case, we have to be careful with selection of the time window, as the AIC picker will always provide a global minimum regardless of whether or not the onset time is included in the selected part of the signal. Moreover, the accuracy of this method depends on SNR. When the signal is contaminated with high-amplitude noises, the global minimum of the AIC function might not correspond with the onset time. For all these reasons, the AIC picker is commonly used in combination with other techniques to guide its work.

Other techniques used are based on polarization analysis (Magotra et al., 1989; Anderson and Nehorai, 1996), artificial neural networks (Gentili and Michelini, 2006; Dai and Macbeth, 1995), fuzzy logic theory (Chu and Mendel, 1994) or wavelets (Galiana-Merino et al., 2008; Mousavi et al., 2016; Bai et al., 2017). Particularly, wavelet analysis has been widely used to denoise the signal or to identify the frequency bands of interest before applying the STA/LTA method (Botella et al., 2003; Galiana-Merino et al., 2007; Gaci, 2014) or the AIC picker (Zhang et al., 2003; Sarout et al., 2009). Thus, for example, Sarout et al. (2009) utilised the wavelet transform to select the frequency band that contains the frequency of the input pulse and, subsequently, they applied the AIC function to estimate the onset time of P-waves for specimens of shale (a fine-grained sedimentary rock) subjected to different confining pressures.

Most of these methods satisfactorily determine P phase arrival when the analysed signals are contaminated with relatively low noise. When the SNR is low and the first arrival is not clear, however, most of them do not perform properly.

In this paper, we have developed a new methodology to automatically estimate the onset time of P and S waves in building rocks. The proposed method works in combination with wavelet analysis initially to improve SNR and runs independently of the frequency of the input pulse. Other works (e.g. Sarout et al., 2009) rely on the frequency of the input pulse to analyse a surrounding frequency band. However, the output signal might differ considerably from the input. The microstructure of the rocks (size and kind of pores, fissures and grains), as well as their geometry affects the amplitude and the waveform of the propagating waves. Specifically, the amplitude decreases and the waveform broadens as the wave propagates (Vidale, 1987; Zhao et al., 2006; Feng and Yi, 2017). Besides, reflection and diffraction effects produce several incoming pulses that distort the correct one. Therefore, detection and characterisation of the first pulse in the output signal might be something not trivial, especially in the case of shear waves. In most of the reported methods, onset time picking does not investigate in the characteristics of the first pulse, therefore other pulses might contaminate the signal and produce false detections. In the proposed method, we analyse all the pulses detected in the output signal, and select the first pulse of the P or S wave according to symmetry, amplitude and duration criteria. This triple check provides greater confidence in the obtained results.

The proposed approach runs automatically and provides the characteristics of the first pulse (amplitude, energy and frequency), as well as the onset time of the P and S waves. It has been tested on twenty-one different types of building rocks. Besides, we have also compared the automatic onset time for S-waves using the special shear wave couplant and the common P-wave couplant. The proposed method reduces human subjectivity, with the aim of increasing the accuracy and repeatability of the onset time estimated for P and S waves.

2. Materials and methods

2.1. Rocks

Twenty-one rock samples were measured, including sedimentary, igneous and metamorphic rocks. These rock types were chosen from among building stones quarried in Spain for their different petrophysical and petrographic characteristics.

We classified the studied rocks according to the following mineralogical and textural properties:

(i) We refer to carbonate rocks (Ca) when the predominant rock-forming minerals are calcite and dolomite (microcrystalline and oolitic limestones, dolostones, calcite and dolomite marbles, biocalcarenites and biocalcirrudites, etc.). In siliceous rocks (Si) the predominant rock-forming minerals are silicates (sandstones, granites, gneiss and syenites).
(ii) We divide the rocks into three classes or textures depending on the particle size: fine-grained (F), where the mean particle diameter is smaller than 0.5 mm; medium-grained (M) with particles 0.5–2 mm; and coarse-grained (C) for particles larger than 2 mm.
(iii) We also classify the studied rock samples into non-porous (nP) and porous (P). The former has porosity values lower than 10%, whereas the latter's porosity is greater than 10%. This porosity threshold comes from the influence of connected porosity on rock properties, including fluid transport, mechanical and durability of rocks. Below 10% porosity, pore connectivity dramatically decreases as a result of the closure and elimination of pore throats. Conversely in rocks of a porosity higher than 10% pore space is well-connected and pore size distribution becomes the most important microstructure parameter (Benavente et al., 2007, 2015).

2.2. Porosity

In this study, we selected porosity as an index property of rocks because it is considered as a key parameter related to rock strength, permeability and durability. Effective porosity, ϕ, was determined using the vacuum water saturation test (UNE-EN, 1936:2007). Dried samples were weighed and placed in a vacuum chamber at 20 ± 7 mbar in order to eliminate any trapped air from the pore system. Distilled water was slowly introduced until the samples were completely covered and, finally, atmospheric pressure was re-established. The saturated and immersed weight of each sample was recorded.

2.3. Elastic waves

The ultrasonic measurements were carried out by means of the transmission method, which consists of two piezoelectric sensors coupled to the sample at constant pressure. Compressive (P) and shear (S) waves were measured using polarised Panametric transducers (1 MHz). Emitting-receiving equipment (Panametrics-NDT 5058PR) and an oscilloscope (TDS 3012B-Tektronix) were used to acquire and digitalize the waveforms to be displayed, manipulated and stored. Two types of visco-elastic couplants were used to achieve good coupling between the transducer and the sample: one of a fluid consistency for the P-wave transducers (eco-gel), and another of a more viscous consistency for the S-waves (SWC, shear wave couplant, GE Panametrics). For practical applications, in this study we also compare the automatic onset time for S-waves using both the special shear wave couplant and the eco-gel P-wave couplant.

Every measurement of the P and S waves was repeated three times in order to test the reproducibility of the experiments and the corresponding results.

We also estimated the spatial attenuation, α, because it is a parameter sensitive to occasional rock defects and also reflects the attenuation processes of elastics waves into the rock. Spatial attenuation is normalized with respect to the distance between the transmitter and receiver sensors (Martinez-Martinez et al., 2011).

Finally, the wavelength, λ, was calculated using the velocity, v, and frequency, f, of the first pulse as $\lambda = v/f$.

2.4. Automatic characterisation of the first pulse

In this work, we have developed a new method for automatic characterisation of the first pulse in both compressional and shear waves. From this characterisation we extract the onset time, amplitude and frequency for each elastic wave and calculate the wave velocity, spatial attenuation and wavelength. In the case of P-waves, the received signal usually has a good SNR. However, in the case of the S-waves, the received signal is distorted by other incoming waves besides the noise. In most of the cases, the P- wave also appears before the S- wave arrivals, which makes manual identification more difficult. In this case ultrasonic couplants play an important role, with notable differences between using a common compressive wave couplant and a special shear wave one. All these circumstances make manual picking of the onset time of the shear wave more confusing even for expert analysts.

In this section we explain in detail the different steps of the automatic process developed, which can be divided in two parts: signal pre-processing, and characterisation of the first pulse (Figs. 1 and 2). The proposed method has been implemented in Matlab, using the Wavelet Toolbox for some steps of the signal pre-processing (see Supplementary Materials). The algorithm might be implemented by the reader in other programming languages with wavelet packages (e.g. Python, R, etc.) according to the following steps of the process explained below. Given a recording signal x(t), the analysis follows the next steps:

2.4.1. Signal pre-processing

Step 1. Removing the continuous or low-frequency disturbances of the recorded signal. In the case of the P-waves, a linear tendency removing is enough. However, in the case of the S-waves, which are more distorted by additional components, we apply a baseline removal based on the Wavelet transform (Galiana-Merino et al., 2013), where Daubechies 10 and level 10 are used as mother wavelet and maximum scale, respectively.

Step 2. Denoising the signal using the Wavelet Packet Transform. All the details about the applied algorithm can be found in Galiana-Merino et al. (2003). For the analysed signals, we select a sample of noise that is between the samples 400 and 1400 (i.e. between 1.6 and 5.6 microseconds). We have used Daubechies 10 and level 6, as mother wavelet and maximum level of decomposition, respectively.

Step 3. Removing the high frequency oscillations. At the beginning of some of the recorded signals some oscillations appear, located around the 10 MHz, which might produce false detections in the time domain. In order to remove these signals, a 2nd order Butterworth low-pass filter has been applied with cut-off frequency at 1 MHz (a tenth below the frequencies that we want to remove).

As result of Steps 1 to 3, we obtain the filtered signal, $x_{Filtered}(t)$, which is the one used for identification of the first arrival.

2.4.2. Characterisation of the first pulse

Once the signal has been cleaned, the pulses contained in the signal were identified and characterised in terms of amplitude, symmetry and duration.

Step 4. Taking the absolute value of the signal $x_{Filtered}(t)$ and normalizing with respect to the maximum, $x_{Abs}(t)$.

Step 5. Calculation of the differences between adjacent samples (i.e. the approximate derivative) and obtain the sign of these differences. In this way, the increasing and decreasing periods of the pulse are transformed into 1 and -1 respectively, given a square pulse signal, $x_{Square}(t)$.

In this case, we are interested in the beginning of the increasing part

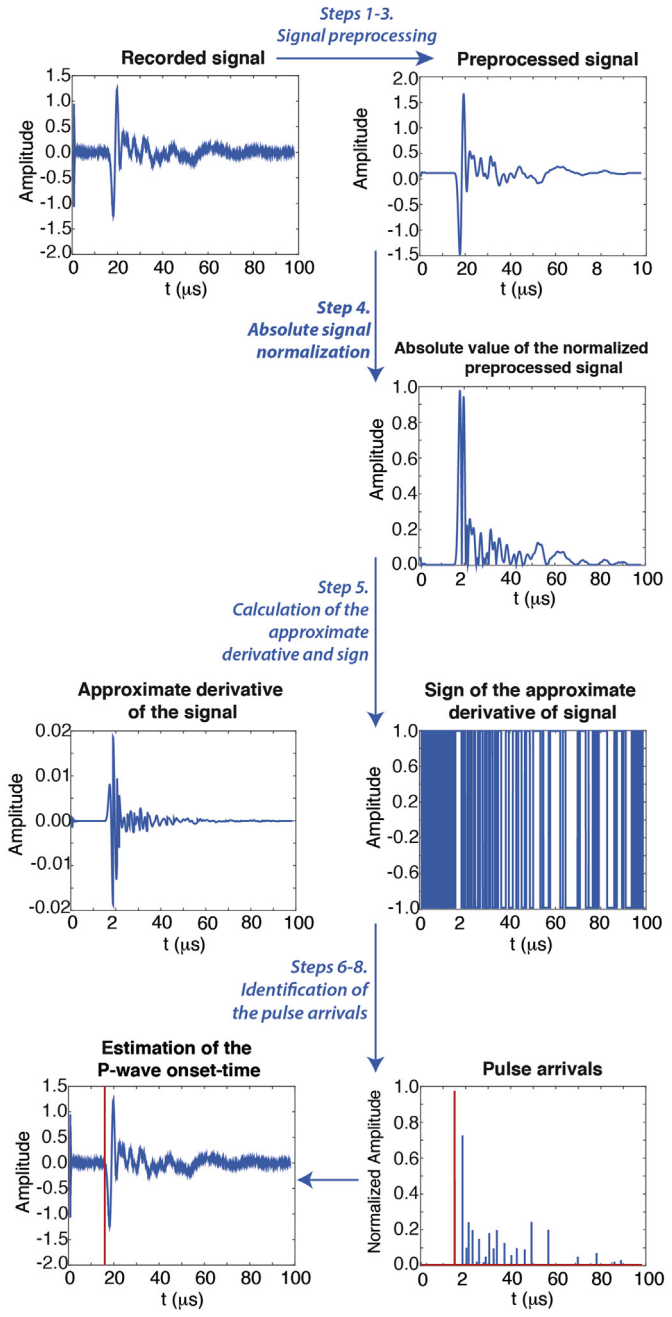

Fig. 1. Example that shows the different steps of the developed automatic process applied to the P-wave signal of CnPSi-21 sample.

of the pulses (i.e. 1). Therefore, after obtaining the square pulse signal, we identify the time intervals where the signal equals to 1, and then the first sample associated to these different sections of the signal. As result, it provides a vector $V_{Arrival}$ with the time associated to the beginning of the different pulses of the signal, that is the time arrivals of all the detected pulses.

Step 6. Analysing the characteristics of the detected pulses in terms of symmetry, amplitude and duration criteria.

For the symmetry study, we obtain firstly the area comprised between two consecutive time arrivals in the signal $x_{Square}(t)$. The area associated to each square pulse is normalized with respect to its length and saved in a vector $V_{Symmetry}$. Since $x_{Square}(t)$ is a square pulse signal between $+1$ and -1, the results will be closer to 0 as more symmetrical is the analysed pulse. Specifically, a value of 0 means a 1:1 ratio between the area corresponding to $+1$ and the area corresponding to -1.

For the amplitude study, the area comprised between two consecutive time arrivals in the signal $x_{Abs}(t)$ was obtained and the result saved in a vector $V_{Amplitude}$. Once obtained the area associated to each pulse, the vector $V_{Amplitude}$ is normalized respecting to the highest value.

Finally, for the duration criterion, the time differences between two consecutive time arrivals were measured and the results saved in a vector $V_{Duration}$.

Step 7. Identifying the first pulse.

Initially, the pulses whose values in $V_{Symmetry}$ and $V_{Duration}$ are above the thresholds $Th_{Symmetry}$ and $Th_{Duration}$, respectively, are ignored, since they are representative of distorted and asymmetric pulses. In the case of the P-wave, the time condition is not required, as the recorded signals usually have a good SNR. After that, the first pulse whose value in $V_{Amplitude}$ is above the established threshold $Th_{Amplitude}$, is defined as the first pulse or first arrival of the signal.

Experimentally, the values of $Th_{Symmetry}$ and $Th_{Amplitude}$ were established at 0.2 and 0.6, respectively. In the case of the $Th_{Symmetry}$, the value of 0.6 corresponds to a 1:4 ratio between the area corresponding to $+1$ and the area corresponding to -1, or vice versa, which provides enough flexibility to the symmetry criterion and takes into consideration the possible distortions due to the arrival of other pulses. Respecting the $Th_{Amplitude}$ parameter, the value of 0.2 allows discarding amplitudes below 20% with respect to the maximum amplitude, which does not imply an extremely restricted margin. Finally, the upper limit, $Th_{Duration}$, related directly to the frequency of the first pulse, has been chosen as 600 samples for the S-wave identification.

Once established these parameters, the P- (or S-) wave detection process is automatic and applicable to all the different kind of rocks analysed in this work.

Step 8. Characterisation of the first pulse.

Once the first pulse has been identified, the difference between the arrival time of this pulse and the subsequent one provides an estimation of the half of the period of the pulse and therefore the frequency, F_{Pulse}. Besides, other parameters as the maximum amplitude, velocity and the energy can be obtained.

Step 9. In the case of the S-waves (Fig. 2), the recorded signals are contaminated with noise and other kind of incoming waves, including the P-wave. In order to refine the estimation of the first arrival carried out in Step 8, the signal $x_{Filtered}(t)$ was band-pass filtered between $F_{Pulse} - 200$ and $F_{Pulse} + 200$ Hz. The band-pass filter used is formed by the series connection between a 2nd order Butterworth low-pass filter with cutoff frequency of $(F_{Pulse} + 200)$ Hz and a 2nd order Butterworth high-pass filter with cutoff frequency of $(F_{Pulse} - 200)$ Hz. As a result we obtain a signal, $x_{Pulse}(t)$, where the first pulse is better defined and less distorted by other waves.

After that, we repeat Steps 4 to 8 with $x_{Pulse}(t)$ and characterise the first pulse of the S-wave.

3. Results and discussion

3.1. P-waves waveform and picking of the onset time

For the studied rocks, the onset time for P-waves was clear and easy to determine, although their waveforms and wavelength values depend on the type of rock. Fig. 3 compares the waveforms of recorded signals for fine, medium and coarse-grained, and porous and non-porous rocks. In particular, P-wave signals have a high signal/noise ratio and their arrival time is clear. Fig. 2 also shows that the frequency of the samples decreases with particle size. Table 1 reports that coarse-grained rocks have the highest wavelength values for the studied rocks. An increase in wavelength hinders manual picking of the onset time for elastic waves, although is less important for P-waves than S-waves.

The obtained P-wave values (Table 1) are similar to those previously published for these types of rocks (Demirdag, 2009). The manual and calculated P-wave values are nearly equal (Fig. 4a). Their discrepancies

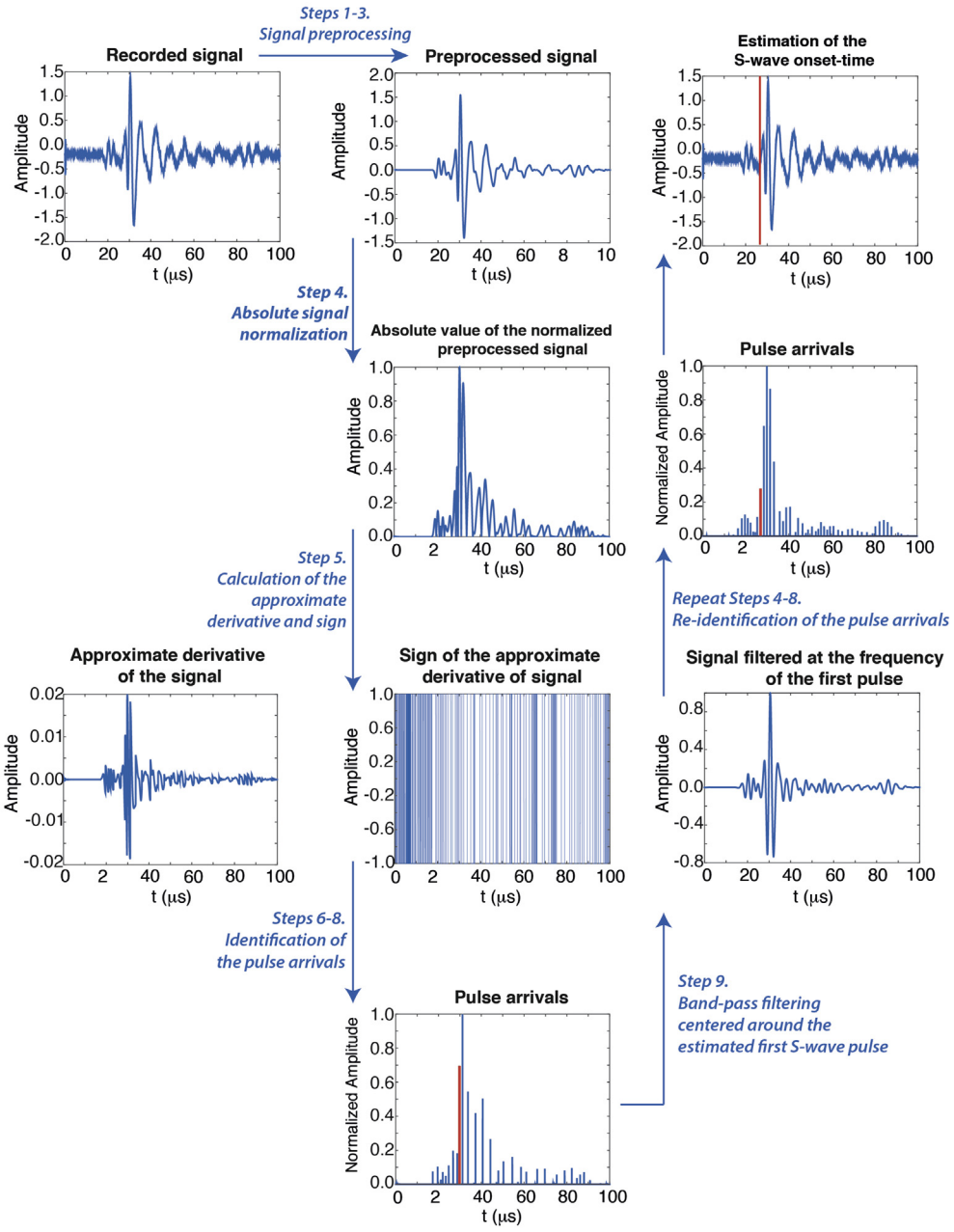

Fig. 2. Example that shows the different steps of the developed automatic process applied to the S-wave signal of CnPSi-21 sample using the special shear wave couplant.

are, on average, around 0.7%, which is within the experimental error of the onset time picking measurements. Sarout et al. (2009) stated that the "true" onset time picking values are intrinsically unknown and, consequently, also the wave velocity values. Most of the published data in the field of rock physics or material characterisation rely on human picking, which includes the subjectivity of the human analyst. Therefore, one may only compare the results of any proposed method to results obtained by a human analyst, without concluding which one is closer to reality. If we consider that manual measurement provides a true or reference value, the proposed method accurately calculates P-waves velocities for the wide variety of studied rocks.

The texture of the rocks affects the velocity and attenuation of the elastic waves and, in the end, picking of the onset time. Fig. 4b relates P-waves velocities and sample porosity. The general trend shows that P-waves velocities decrease as rock porosity values increase. This logical and well-known relationship is due to the fact that propagation of ultrasonic waves is more difficult in samples with a high pore fraction. However, there is a cluster of points that clearly are out of the general trend. This cluster corresponds mainly to those rocks with low porosity (around 1.5%) and medium-coarse crystal size. This particular behaviour in the velocity-porosity trend for these types of rocks has been observed previously (Garcia-del-Cura et al., 2012; Martinez-Martinez et al., 2016; Benavente et al., 2018). These workers concluded that crystal size has a significant influence on ultrasonic wave velocity, where crystal edges cause a strong wave scattering. In addition to porosity and crystal size, mineralogical composition of rocks also has an important influence on ultrasonic wave velocity. Thus, for example, quartz and feldspar lead to lower elastic wave values than calcite and dolomite (Schön, 2011).

Fig. 4c shows a direct relationship between spatial attenuation and porosity, and highlights that porous and non-porous rocks have a different pattern, in common to the P-wave velocities. Spatial attenuation

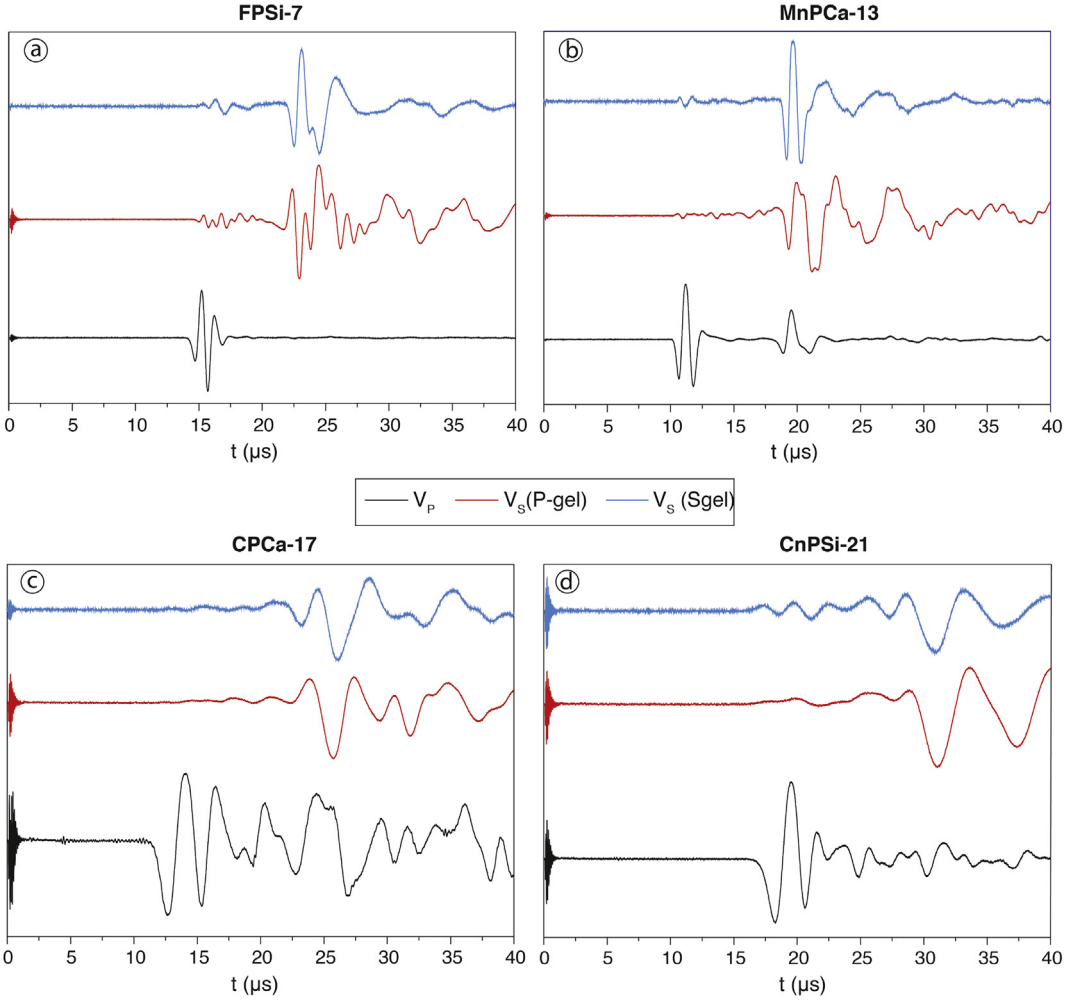

Fig. 3. P- and S-wave signals for porous and non-porous rocks with a fine, medium and coarse particle size using the compressive wave (P-gel) and the special shear wave (S-gel) couplants.

increases with porosity because pores reflect, scatter and absorb elastic waves. These processes are important for coarse-grained porous rocks in the same manner as for coarse-grained non-porous rocks. The presence of coarse particles causes efficiently high wave reflections and scattering compared to fine and medium particles.

Microstructural components of the rocks such as pores, fissures and grains act as a wavelength filter and the output signals have different wavelengths depending on the grain size. Table 1 and Fig. 4d highlight that coarse-grained rocks have the highest wavelength value. Although the central frequency of the input elastic waves is fixed at 1 MHz, the frequency of first pulse of the output signal differs as a consequence of elastic wave interactions with the microstructural components of the rocks (from 0.1–0.6 MHz). These results reveal the importance of characterisation of the frequency components of the output rather than the input signal. The microstructural components of each sample cause a unique although complex interaction with the elastic waves that define the resultant output waveform. Coarse-grained rocks have the highest waveform attenuation and wavelength and, consequently, they make manual picking of the onset time for elastic waves more difficult.

3.2. S-waves waveform and picking of the onset time

The onset time for S-waves was picked using the special shear wave couplant. For the studied rocks, manual picking of the onset time was clearly achieved for fine-grained rocks. As the particle size increases, picking of the onset time becomes more difficult and time-consuming. Different S-waveform problems can be highlighted for medium to coarse-grained rocks: the contamination of S-waveforms by P-waves, the reduction of waveform amplitude (lower SNR) and increase of wavelength. Fig. 3 compares S-waveforms for selected rocks with different particle sizes. For coarse-grained rocks, S-waveforms are noisy (low SNR) in the waveform zone from P -wave and S-wave arrivals due to the presence of remaining P-waves. As in the P-waves, coarse-grained rocks show the highest attenuation and S-wavelength values (Table 1).

In spite of these problems, S-wave velocity values agree with published data for similar rocks, and we can consider the manually measured as “true” or reference values. Fig. 5 compares manual and calculated S-wave values and shows that the proposed methodology accurately obtains S-wave velocity values for the studied rocks. The discrepancies between manual and automatic procedures are, on average, around 4.4%, which is within the experimental error of the onset time picking measurements. In general, the automatic method obtains V_S values slightly higher than manual method (Table 1).

The proposed methodology has the advantage of distinguishing between the remaining P-waves and S-waves using the symmetry, amplitude and duration criteria described in section 3, in contrast to subjectivity of the human analyst. Moreover, our results show that the frequency of the main peak corresponding to the P and S waves is different (Table 1), and represents an additional differentiating characteristic. The use of the proposed methodology is therefore recommended for medium to coarse-grained rocks, where the quality of the S-waveform signals are poor and manual picking of the onset time

Table 1
Properties and elastic waves parameters of the studied rocks. Reference includes information on the mineralogy (carbonate, Ca, and siliceous, Si, rocks), particle size (medium, M, coarse, C, and fine-grained, F) and porosity (non-porous, nP, and porous, P, rocks). Mean values and coefficient of variation (CV) of porosity (ϕ) and P- (V_P) and S-wave (V_S) velocities obtained manually (manual) and automatically (autom), spatial attenuation, α, and wavelength, λ. S-waves were taken using both the especial shear-wave (S-gel) and common compressive-wave couplants (P-gel).

Rock				Compressional waves				Shear waves					
Reference	Rock classification	Particle Size	ϕ (%)	v_P, manual (m/s)	v_P, autom (m/s)	α (dB/cm)	λ (mm)	v_S, manual (m/s)	v_S, S-gel (m/s)	CV (%)	λ (mm)	v_S, P-gel (m/s)	CV (%)
FPCa-1	Biocalcarenite (sedimentary)	Fine	16.29	3656	3638	6.99	8.09	2146	2179	3.78	6.78	2259	2.46
FPCa-2	Biocalcarenite (sedimentary)	Fine	20.61	3702	3697	7.41	7.90	2186	2313	0.32	6.87	2272	0.50
FPCa-3	Biocalcarenite (sedimentary)	Fine	22.03	3619	3616	8.54	9.03	2354	2158	0.68	6.75	2225	1.95
FPCa-4	Biocalcarenite (sedimentary)	Fine	16.70	3653	3650	6.59	8.18	2234	2356	0.94	5.19	2350	0.32
FPCa-5	Dolostone (sedimentary)	Fine	18.87	3805	3821	6.95	7.58	2424	2504	0.34	5.52	2393	2.77
FPCa-6	Dolostone (sedimentary)	Fine	17.13	3896	3913	6.91	7.98	2430	2548	0.38	5.26	2498	1.04
FPSi −7	Sandstone (sedimentary)	Fine	13.11	4219	4225	7.63	7.61	2721	2784	0.33	4.76	2812	1.13
FPSi-8	Sandstone (sedimentary)	Fine	16.05	3120	3130	8.30	9.67	2042	2130	0.55	7.24	2112	2.71
FnPCa-9	Microcrystalline limestone (sedimentary)	Fine	1.30	5948	6078	7.27	10.06	3164	3382	0.76	6.95	4307	27.73
FnPCa-10	Microcrystalline limestone (sedimentary)	Fine	1.37	5962	6031	7.34	11.19	3229	3173	4.23	6.78	4306	4.85
MPCa-11	Oolitic limestone (sedimentary)	Medium	8.62	5621	5666	4.23	10.74	3067	3251	0.17	6.16	3193	1.89
MPCa-12	Oolitic limestone (sedimentary)	Medium	10.62	5165	5250	3.84	9.03	2872	3021	0.26	5.07	2995	0.37
MnPCa-13	Oolitic limestone (sedimentary)	Medium	5.44	5853	5907	3.52	10.30	3135	3296	0.09	5.33	3430	16.65
MnPCa-14	Dolomite marble (metamorphic)	Medium	1.48	3213	3237	8.24	12.25	2337	2391	2.50	6.80	2916	2.36
MnPCa-15	Calcite marble (metamorphic)	Medium	0.90	5317	5363	7.79	13.30	3016	3012	6.00	6.57	3315	0.55
MnPSi-16	Granite (igneous)	Medium	1.99	5429	5503	6.16	11.31	3311	3432	2.19	5.89	4165	1.28
CPCa-17	Biocalcirrudite (sedimentary)	Coarse	20.35	4880	4878	11.51	20.45	2254	2398	2.66	11.19	2654	2.81
CPCa-18	Biocalcirrudite (sedimentary)	Coarse	19.01	4905	4906	9.70	13.89	2700	2630	3.00	7.12	2602	3.63
CnPCa-19	Calcite marble (metamorphic)	Coarse	0.68	5833	5860	9.59	15.38	2498	2727	4.75	16.20	2614	5.40
CnPSi-20	Syenite (igneous)	Coarse	1.98	3119	3082	10.83	30.77	2468	2609	0.23	19.53	2559	1.65
CnPSi-21	Gneiss (metamorphic)	Coarse	1.65	3608	3647	9.37	17.62	2168	2125	4.60	7.16	2141	0.88

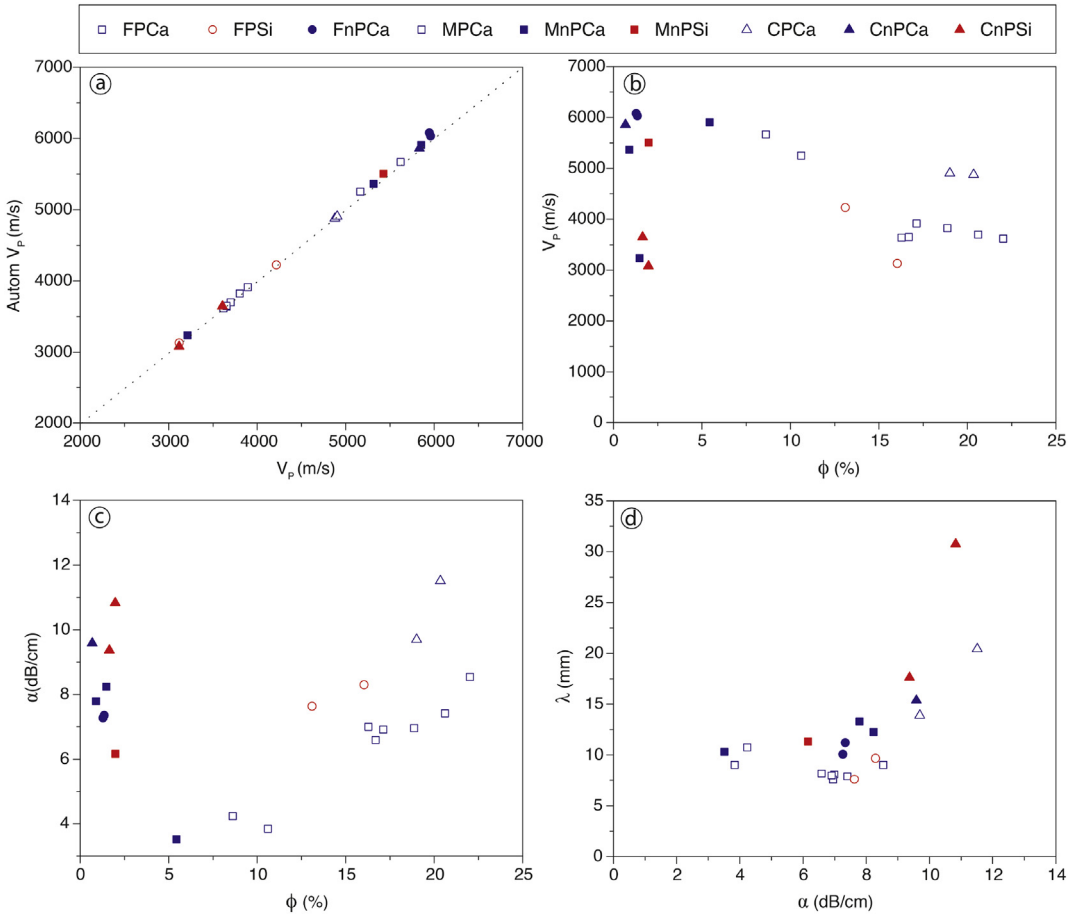

Fig. 4. Relation between porosity (ϕ) and P-wave parameters: P-wave velocity (V_P) obtained manually (manual) and automatically (autom), spatial attenuation, α, and wavelength, λ.

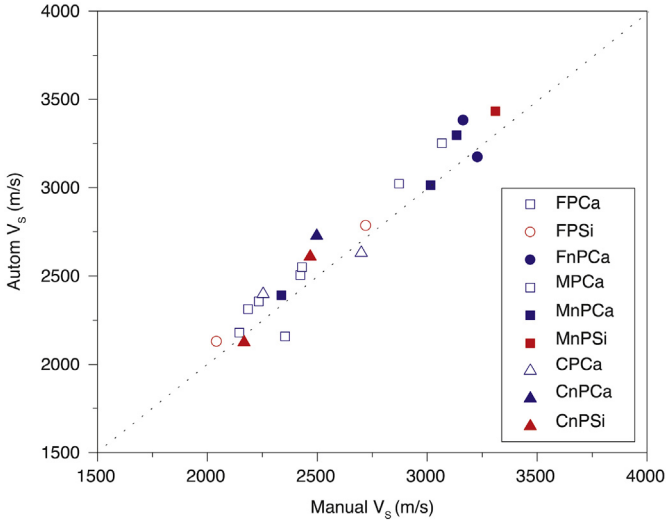

Fig. 5. Comparison of S-wave velocities (V_S) obtained manually (manual) and automatically (autom) using the special shear wave couplant (S-gel).

becomes more difficult and time consuming.

For practical applications, we also compare the automatic onset time for S-waves obtained using both types of transducer couplants: the special shear wave couplant and the common compressive wave couplant (those usually used for P-waves studies). Fig. 6 shows S-wave velocity values for manual and automatic methodologies. For most of the studied rocks, S-wave velocity values using the common compressive wave couplant are similar to the manual ones. Porous rocks give the best results (Fig. 6a) whereas the major discrepancies between the S-wave velocity values are found for some non-porous rocks independently of their grain size (Fig. 6b). Although our automatic methodology has yielded promising results, more research is needed to improve picking of the onset time without using the special shear wave couplant. These findings have practical applications, for example in stone conservation studies, where the removal and cleaning of the material surface after application of the common couplant is more effective and harmless than using the special shear wave couplant.

4. Conclusions

This paper addresses determination of the picking of the onset of P- and S- waves in transmitted output waveforms. Results confirm that our proposed methodology provides precise values of the onset time of P- and S- waves. The great advantage of this methodology is the accuracy and repeatability of the obtained results, which do not depend on human subjectivity.

The proposed methodology has been successfully applied to a wide variety of sedimentary, igneous and metamorphic building rocks. The recorded signals show that the microstructural components of rock have a strong influence on the output signal. Although the central frequency of the input elastic pulses is fixed at 1 MHz, the frequency and wavelength of the first pulse in the output signal, and the signal attenuation, noticeably vary with mineralogy, porosity and particle size. Consequently, accurate determination of the arrival time of the P- and S- waves requires characterisation of the frequency components of the output rather than the input signal. Furthermore, these complex interactions between the elastic waves and the microstructural components of rocks particularly affect manual picking of the onset time in coarse-grained rocks, which have the highest waveform attenuation and wavelength.

For the studied rocks, P-wave signals yield a high SNR and their arrival-time is clear and easy to determine. The discrepancies between automatic and manual measurements are, on average, around 0.7%, which is within the experimental error of the onset time picking measurements. Mineralogy, porosity and particularly particle size of rocks affects the wavelength, velocity and attenuation of the P- waves and, in the end, picking of the onset time. An increase in the wavelength hinders manual picking of the onset time for elastic waves, although is less important for P-waves than S-waves.

Determination of the arrival time of S- waves presents critical problems in case of medium to coarse-grained rocks: the contamination of S-waveforms by P-waves, the reduction of the waveform amplitude (lower SNR) and the increase of wavelength. Consequently, manual picking of onset time becomes more difficult and time-consuming. The proposed methodology, however, distinguishes between the remaining P-waves and S-waves independently of the human analyst. In general, the automatic method obtains V_S values slightly higher than the manual method and their discrepancies are, on average, around 4.4%.

Finally, the determination of automatic onset time for S-waves using common P-wave couplant has shown promising results. It presents practical applications that could avoid the use of the special shear wave couplant for the picking of the onset time of S- waves.

Acknowledgements

This work was supported by the Spanish Government [grant number RTI2018-099052-B-I00], Regional Government of Comunidad Valenciana (Spain) [grant number AICO/2016/098] and Madrid (Spain) [Top Heritage, grant number S2018/NMT-4372] and the University of Alicante [grant number GRE17-12]. Predoctoral fellowships were awarded to D. Crespo-Jimenez by the MEFP [FPU2017/04377 and BDNS 311327]. Special thanks to Prof. Martin Lee for his

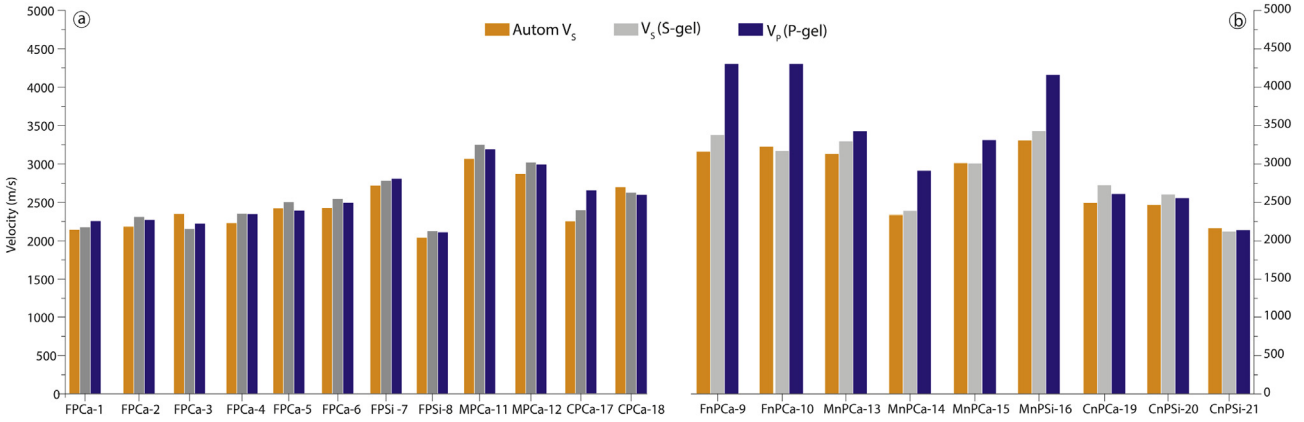

Fig. 6. Comparison of the S-wave velocities (V_S) obtained manually (manual) and automatically (autom) using the special shear wave couplant (S-gel) for porous (a) and non-porous (b) rocks.

valuable comments and suggestions.

Declaration of Competing Interests

The authors declare that they have no known competing financial interests or personal relationships that could have appeared to influence the work reported in this paper.

Appendix A. Supplementary data

Supplementary data to this article can be found online at https://doi.org/10.1016/j.enggeo.2020.105474.

References

Akaike, H., 1974. Markovian representation of stochastic-processes and its application to analysis of autoregressive moving average processes. Ann. Inst. Stat. Math. 26, 363–387. https://doi.org/10.1007/BF02479833.

Allen, R.V., 1978. Automatic earthquake recognition and timing from single traces. Bull. Seismol. Soc. Am. 68, 1521–1532.

Anderson, S., Nehorai, A., 1996. Analysis of a polarized seismic wave model. IEEE Trans. Signal Process. 44, 379–386. https://doi.org/10.1109/78.485933.

Bai, F., Gagar, D., Foote, P., Zhao, Y., 2017. Comparison of alternatives to amplitude thresholding for onset detection of acoustic emission signals. Mech. Syst. Signal Process. 84, 717–730. https://doi.org/10.1016/j.ymssp.2016.09.004.

Benavente, D., Cueto, N., Martinez-Martinez, J., Garcia del Cura, M.A., Canaveras, J.C., 2007. The influence of petrophysical properties on the salt weathering of porous building rocks. Environ. Geol. 52, 197–206. https://doi.org/10.1007/s00254-006-0475-y.

Benavente, D., Pla, C., Cueto, N., Galvan, S., Martinez-Martinez, J., Garcia-del-Cura, M.A., Ordonez, S., 2015. Predicting water permeability in sedimentary rocks from capillary imbibition and pore structure. Eng. Geol. 195, 301–311. https://doi.org/10.1016/j.enggeo.2015.06.003.

Benavente, D., Martinez-Martinez, J., Cueto, N., Ordonez, S., Garcia-del-Cura, M.A., 2018. Impact of salt and frost weathering on the physical and durability properties of travertines and carbonate tufas used as building material. Environ. Earth Sci. 77, 147. https://doi.org/10.1007/s12665-018-7339-0.

Botella, F., Rosa-Herranz, J., Giner, J.J., Molina, S., Galiana-Merino, J.J., 2003. A real-time earthquake detector with prefiltering by wavelets. Comput. Geosci. 29, 911–919. https://doi.org/10.1016/S0098-3004(03)00099-2.

Brotons, V., Tomas, R., Ivorra, S., Grediaga, A., Martínez-Martínez, J., Benavente, D., Gómez-Heras, M., 2016. Improved correlation between the static and dynamic elastic modulus of different types of rocks. Mater. Struct. 49, 3021. https://doi.org/10.1617/s11527-015-0702-7.

Carpinteri, A., Xu, J., Lacidogna, G., Manuello, A., 2012. Reliable onset time determination and source location of acoustic emissions in concrete structures. Cem. Concr. Compos. 34, 529–537. https://doi.org/10.1016/j.cemconcomp.2011.11.013.

Chu, C., Mendel, J.M., 1994. First break refraction event picking using fuzzy-logic systems. IEEE Trans. Fuzzy Syst. 2, 255–266. https://doi.org/10.1109/91.324805.

Dai, H.C., Macbeth, C., 1995. Automatic picking of seismic arrivals in local earthquake data using an artificial neural-network. Geophys. J. Int. 120, 758–774. https://doi.org/10.1111/j.1365-246X.1995.tb01851.x.

Demirdag, S., 2009. The effect of using different polymer and cement based materials in pore filling applications on technical parameters of travertine stone. Constr. Build. Mater. 23, 522–530. https://doi.org/10.1016/j.conbuildmat.2007.10.019.

Earle, P.S., Shearer, P.M., 1994. Characterization of global seismograms using an automatic-picking algorithm. Bull. Seismol. Soc. Am. 84, 366–376.

Feng, H., Yi, W., 2017. Propagation characteristics of acoustic emission wave in reinforced concrete. Results Phys. 7, 3815–3819. https://doi.org/10.1016/j.rinp.2017.09.060.

Gaci, S., 2014. The use of Wavelet-based denoising techniques to enhance the first-arrival picking on seismic traces. IEEE Trans. Geosci. Remote Sens. 52, 4558–4563. https://doi.org/10.1109/TGRS.2013.2282422.

Galiana-Merino, J.J., Rosa-Herranz, J., Giner, J., Molina, S., Botella, F., 2003. De-noising of short-period seismograms by wavelet packet transform. Bull. Seismol. Soc. Am. 93 (6), 2554–2562. https://doi.org/10.1785/0120010133.

Galiana-Merino, J.J., Rosa-Herranz, J., Jauregui, P., Molina, S., Giner, J., 2007. Wavelet transform methods for azimuth estimation in local three-component seismograms. Bull. Seismol. Soc. Am. 97, 793–803. https://doi.org/10.1785/0120050225.

Galiana-Merino, J.J., Rosa-Herranz, J., Parolai, S., 2008. Seismic P phase Picking using a kurtosis-based Criterion in the stationary wavelet domain. IEEE Trans. Geosci. Remote Sens. 46, 3815–3826. https://doi.org/10.1109/TGRS.2008.2002647.

Galiana-Merino, J.J., Rosa-Herranz, J.L., Rosa-Cintas, S., Martinez-Espla, J.J., 2013. SeismicWaveTool: continuous and discrete wavelet yyysis and filtering for multi-channel seismic data. Comput. Phys. Commun. 184, 162–171. https://doi.org/10.1016/j.cpc.2012.08.008.

Garcia-del-Cura, M.A., Benavente, D., Martinez-Martinez, J., Cueto, N., 2012. Sedimentary structures and physical properties of travertine and carbonate tufa building stone. Constr. Build. Mater. 28, 456–467. https://doi.org/10.1016/j.conbuildmat.2011.08.042.

Gentili, S., Michelini, A., 2006. Automatic picking of P and S phases using a neural tree. J. Seismol. 10, 39–63. https://doi.org/10.1007/s10950-006-2296-6.

Hamdi, E., Lathaj, Z., 2013. Microcracking based rock classification using ultrasonic and porosity parameters and multivariate analysis methods. Eng. Geol. 167, 27–36. https://doi.org/10.1016/j.enggeo.2013.10.008.

Kurz, J.H., Grosse, C.U., Reinhardt, H.W., 2005. Strategies for reliable automatic onset time picking of acoustic emissions and of ultrasound signals in concrete. Ultrasonics 43, 538–546. https://doi.org/10.1016/j.ultras.2004.12.005.

Lee, M., Byun, J., Kim, D., Choi, J., Kim, M., 2017. Improved modified energy ratio method using a multi-window approach for accurate arrival picking. J. Appl. Geophys. 139, 117–130. https://doi.org/10.1016/j.jappgeo.2017.02.019.

Leonard, M., 2000. Comparison of manual and automatic onset time picking. Bull. Seismol. Soc. Am. 90, 1384–1390. https://doi.org/10.1785/0120000026.

Magotra, N., Ahmed, N., Chael, E., 1989. Single-station seismic event detection and location. IEEE Trans. Geosci. Remote Sens. 27, 15–23. https://doi.org/10.1109/36.20270.

Martinez-Martinez, J., Benavente, D., Garcia-del-Cura, M.A., 2011. Spatial attenuation: the most sensitive ultrasonic parameter for detecting petrographic features and decay processes in carbonate rocks. Eng. Geol. 119, 84–95. https://doi.org/10.1016/j.enggeo.2011.02.002.

Martinez-Martinez, J., Benavente, D., Gomez-Heras, M., Marco-Castano, L., Garcia-del-Cura, M.A., 2013. Non-linear decay of building stones during freeze-thaw weathering processes. Constr. Build. Mater. 38, 443–454. https://doi.org/10.1016/j.conbuildmat.2012.07.059.

Martinez-Martinez, J., Fusi, N., Galiana-Merino, J.J., Benavente, D., Crosta, G.B., 2016. Ultrasonic and X-ray computed tomography characterization of progressive fracture damage in low-porous carbonate rocks. Eng. Geol. 200, 47–57. https://doi.org/10.1016/j.enggeo.2015.11.009.

Mousavi, S.M., Langston, C.A., Horton, S.P., 2016. Automatic microseismic denoising and onset detection using the synchrosqueezed continuous wavelet transform. Geophysics 81, V341–V355. https://doi.org/10.1190/GEO2015-0598.1.

Sarout, J., Ferjani, M., Gueguen, Y., 2009. A semi-automatic processing technique for elastic-wave laboratory data. Ultrasonics 49, 452–458. https://doi.org/10.1016/j.ultras.2008.12.001.

Schön, J.H., 2011. Physical Properties of Rocks: Fundamentals and Principles of Petrophysics. Handbook of Geophysical Exploration, second ed. Elsevier, Oxford.

Sleeman, R., van Eck, T., 1999. Robust automatic P-phase picking: an on-line implementation in the analysis of broadband seismogram recordings. Phys. Earth Planet. Inter. 113, 265–275. https://doi.org/10.1016/S0031-9201(99)00007-2.

UNE-EN, 1936. 2007. Natural Stone Test Method. Determination of Real Density and Apparent Density, and of Total and Open Porosity. European Committee for Standardization, Bruxelles.

Vidale, J.E., 1987. Wave-Form Effects of a High-Velocity, Subducted Slab. Geophys. Res. Lett. 14, 542–545. https://doi.org/10.1029/GL014i005p00542.

Wang, Q., Ji, S., Sun, S., Marcotte, D., 2009. Correlations between compressional and shear wave velocities and corresponding Poisson's ratios for some common rocks and sulfide ores. Tectonophysics 469, 61–72. https://doi.org/10.1016/j.tecto.2009.01.025.

Withers, M., Aster, R., Young, C., Beiriger, J., Harris, M., Moore, S., Trujillo, J., 1998. A comparison of select trigger algorithms for automated global seismic phase and event detection. Bull. Seismol. Soc. Am. 88, 95–106.

Zhang, H.J., Thurber, C., Rowe, C., 2003. Automatic P-wave arrival detection and picking with multiscale wavelet analysis for single-component recordings. Bull. Seismol. Soc. Am. 93, 1904–1912. https://doi.org/10.1785/0120020241.

Zhao, J., Cai, J.G., Zhao, X.B., Li, H.B., 2006. Experimental study of ultrasonic wave attenuation across parallel fractures. Geomech. Geoengin. 1, 87–103. https://doi.org/10.1080/17486020600834613.